

Hydration of Amino Acid Side Chains: Nonpolar and Electrostatic Contributions Calculated from Staged Molecular Dynamics Free Energy Simulations with Explicit Water Molecules

Yuqing Deng and Benoît Roux*

Biochemistry Department, Weill Medical College of Cornell University, 1300 York Avenue, New York, New York 10021

Received: April 5, 2004; In Final Form: July 20, 2004

A staged protocol for performing molecular dynamics solvation free energy simulations is described. The solvation free energy is expressed in terms of nonpolar and electrostatic contributions, and the nonpolar contribution is further decomposed into repulsive and dispersive contributions using the Weeks, Chandler, and Andersen (WCA) scheme of separating the repulsive and attractive parts in the Lennard-Jones potential. To achieve precise and stable results in the free energy perturbation simulations, the contribution to the free energy from the repulsive part of the potential is computed in multiple stages via a soft-core transformation, whereas a linear coupling scheme is used for both the electrostatic and dispersive contributions. To reduce the computational effort, the free energy simulations are carried out with a small number of explicit solvent water molecules near the solute, whereas the influence of the remaining bulk solvent is represented implicitly in terms of an effective solvent boundary potential. The protocol is used to calculate the hydration free energy of amino acid side chains. Because all of the sampling windows are generated independently of one another, the calculations can all be performed simultaneously in parallel on a computer cluster. The agreement with experimental values and with the high precision computational results of Shirts et al. [*J. Chem. Phys.* **2003**, *119*, 5740] shows that this computationally inexpensive protocol is efficient.

I. Introduction

A quantitative determination of solvation free energies is a problem of central importance in theoretical biophysics.^{1,2} In particular, solvation effects have profound influences on the conformational stability and folding of proteins and on molecular recognition phenomena involving the association of ligands to macromolecules with high affinity and specificity.^{3–7} To understand such thermodynamically driven biological processes, one must be able to account accurately for the solvation free energies arising in diverse and complex environments.

Intermolecular forces consist of short-range harsh repulsive interactions, arising from Pauli's exclusion, van der Waals attraction,⁸ arising from quantum mechanical dispersion, and long-range electrostatic interactions. In standard biomolecular potential functions,^{9–11} the nonpolar repulsion and dispersion forces are modeled with Lennard-Jones (LJ) potentials, whereas electrostatic forces are represented as coulomb interactions between partial charges. Such a separation of the intermolecular forces is useful for decomposing the solvation free energy of a molecular solute into distinct contributions. The total solvation free energy of a molecular solute, ΔG^{tot} , may be formally expressed as the total reversible thermodynamic work needed to sequentially "switch on", in a step-by-step process, the solute–solvent nonpolar and electrostatic interactions, yielding ΔG^{np} , and ΔG^{elec} , respectively.¹² The total solvation free energy is then $\Delta G^{\text{tot}} = \Delta G^{\text{np}} + \Delta G^{\text{elec}}$. Although any decomposition of the solvation free energy is by definition path-dependent,¹³ an analysis based on the step-by-step reversible work provides a useful framework for understanding the nature of solvation

because each individual contribution can be constructed to correspond to microscopic processes with a clear and well-defined physical meaning.¹⁴ For example, the work needed to switch on the solute–solvent electrostatic interactions, ΔG^{elec} , corresponds to the charging free energy of the solute, a quantity that finds its direct correspondence in macroscopic continuum electrostatics.¹⁴

Although the fundamental nature of the intermolecular forces governing the solvation free energy is relatively well-understood, designing efficient and accurate computational schemes remains a challenge. In principle, free energy perturbation (FEP) calculations based on molecular dynamics (MD) simulations of atomic models including explicitly a large number of solvent molecules provide the most detailed representation. Although certainly possible, carrying out such MD/FEP all-atom explicit solvent simulations using the standard periodic boundary conditions (PBC) methodology remains computationally intensive¹⁵ and becomes rapidly prohibitive if a very large number of compounds (hundreds and even thousands) must be examined. Trying to avoid explicit solvent simulations altogether and to achieve computational efficiency, a number of approximate schemes have been developed to incorporate the dominant effects of solvent implicitly (i.e., without including any explicit solvent molecules). The nonpolar contribution is often approximated by the solvent-accessible surface area S (SASA), with $\Delta G^{\text{np}} = \gamma S$, where γ is some empirical surface tension of the solvent, whereas the electrostatic contributions ΔG^{elec} is often approximated by representing the solvent as a structureless dielectric continuum^{16,17} (see also ref 14 for a review).

It is important to seek ways to decrease the computational cost of MD/FEP calculations with explicit solvent molecules

* To whom correspondence should be addressed.

while keeping them accurate. Although implicit solvent models and simplified scoring schemes are very useful, a representation in which all atomic and structural details of the solvent molecules are ignored may not always be appropriate. Ultimately, one would like to have the ability to use MD/FEP routinely as a tool, for example, to screen large databases and identify potential drug lead molecules. To reduce the computational cost of the calculations as much as possible, the systems are simulated with a limited number of explicit water molecules in the vicinity of the solute, while the influence of the remaining bulk is incorporated via an effective spherical solvent boundary potential (SSBP).¹⁸

Our goal is to design a robust MD/FEP computational scheme for rapid and accurate calculations of the solvation free energy of biomolecular solutes with explicit water molecules. To provide further insight into the nonpolar contribution to the solvation free energy, the LJ potential is separated into purely repulsive and attractive parts using the scheme originally developed by Weeks, Chandler, and Andersen (WCA) in the context of liquid perturbation theory.¹⁹ According to the WCA scheme, the LJ potential is split into purely repulsive (force and energy are positive), and attractive (force and energy are negative) parts. By construction, the WCA separation guarantees that the free energy associated with introducing the repulsive part of the solute–solvent potential is positive definite, whereas the free energy associated with introducing the attractive part of the solute–solvent potential is negative definite. This suggests that the evaluation of the nonpolar free energy contributions might benefit from the WCA decomposition of the repulsive and attractive forces. Furthermore, recent investigations^{12,17} have shown that similar decomposition of the nonpolar free energy into repulsive and dispersive contributions is very advantageous to better understand the factors governing hydrophobic solvation and protein stability.

In the current strategy, the free energy contributions from the LJ-WCA core repulsion, the LJ-WCA dispersive attraction, and electrostatic Coulomb interactions are calculated separately according to a staging procedure. To avoid problems associated with the insertion of the solute into the solvent, a nonlinear transformation of the LJ-WCA repulsion to a soft-core potential is used in MD/FEP. Linear scaling is used for the other contributions. In the next section, the formal aspect of the theory is elaborated and the staged free energy simulation protocol is presented. The simulation protocol is then illustrated with the calculation of the hydration free energy of amino acid side chains for both the CHARMM and AMBER force field and comparison with the high precision calculations of Shirts et al.¹⁵

II. Theory

A. Decomposition of the Solvation Free Energy. Let us consider the solvation of a single solute molecule (“u”) into a molecular solvent (“v”). The coordinates of the solute are represented by \mathbf{X} and the coordinates of all the solvent molecules are collectively represented by \mathbf{Y} . To facilitate further development, the total potential energy, $U(\mathbf{X}, \mathbf{Y})$, is expressed as

$$U(\mathbf{X}, \mathbf{Y}) = U_u(\mathbf{X}) + U_v(\mathbf{Y}) + U_{uv}(\mathbf{X}, \mathbf{Y}) \quad (1)$$

where U_u is the internal potential energy of the solute molecule, U_v is the total solvent potential energy, and U_{uv} is the interaction between the solute and solvent molecules. At infinite dilution, the solvation free energy is the total reversible thermodynamic work performed as a single solute molecule is transferred from the gas phase to a pure bulk solvent phase. In the canonical

ensemble, the total reversible work ΔG^{tot} is equivalent to the excess chemical potential²⁰

$$\Delta G^{\text{tot}} = -\frac{1}{\beta} \ln \left[\frac{\int d\mathbf{X} d\mathbf{Y} e^{-\beta U(\mathbf{X}, \mathbf{Y})}}{\int d\mathbf{Y} e^{-\beta U_v(\mathbf{Y})} \int d\mathbf{X} e^{-\beta U_u(\mathbf{X})}} \right] \quad (2)$$

where $\beta = 1/k_B T$. Typically, the solute–solvent interaction potential, $U_{uv}(\mathbf{X}, \mathbf{Y})$, comprises a short-range nonpolar contribution and a long-range electrostatic contribution

$$U_{uv}(\mathbf{X}, \mathbf{Y}) = U_{uv}^{\text{np}}(\mathbf{X}, \mathbf{Y}) + U_{uv}^{\text{elec}}(\mathbf{X}, \mathbf{Y}) \quad (3)$$

Such a separation of the potential energy leads naturally to a decomposition of the solvation free energy¹⁴

$$\Delta G^{\text{tot}} = \Delta G^{\text{np}} + \Delta G^{\text{elec}} \quad (4)$$

where

$$\Delta G^{\text{np}} = -\frac{1}{\beta} \ln \left[\frac{\int d\mathbf{X} d\mathbf{Y} e^{-\beta [U_u(\mathbf{X}) + U_v(\mathbf{Y}) + U_{uv}^{\text{np}}(\mathbf{X}, \mathbf{Y})]}}{\int d\mathbf{Y} e^{-\beta U_v(\mathbf{Y})} \int d\mathbf{X} e^{-\beta U_u(\mathbf{X})}} \right] \quad (5)$$

and

$$\Delta G^{\text{elec}} = -\frac{1}{\beta} \ln \left[\frac{\int d\mathbf{X} d\mathbf{Y} e^{-\beta U(\mathbf{X}, \mathbf{Y})}}{\int d\mathbf{X} d\mathbf{Y} e^{-\beta [U_u(\mathbf{X}) + U_v(\mathbf{Y}) + U_{uv}^{\text{np}}(\mathbf{X}, \mathbf{Y})]}} \right] \quad (6)$$

The nonpolar interactions include both a harsh core–core solute–solvent repulsion and a slow-varying van der Waals solute–solvent dispersive attraction. These two starkly contrasted interactions contribute to the solvation free energy in drastically different ways. In particular, the core repulsion gives rise to an unfavorable free energy corresponding to the thermodynamic work needed to create an empty cavity for accommodating the solute in the bulk solvent. On the other hand, the van der Waals dispersion attraction gives rise to a favorable contribution to the solvation free energy. Previous studies have indicated that the contributions from the repulsive and dispersive interactions to the total nonpolar free energy oppose one another and nearly cancel out.^{22,21} Our understanding of the microscopic factors governing the solvation free energy of a molecular solute is aided by a further decomposition of the nonpolar free energy into purely repulsive and dispersive contributions. In most biomolecular force fields,^{9–11} the nonpolar interaction is represented by the LJ 12–6 pairwise potential

$$u_{ij}^{\text{LJ}}(r) = \epsilon_{ij} \left[\left(\frac{R_{ij}^*}{r} \right)^{12} - 2 \left(\frac{R_{ij}^*}{r} \right)^6 \right] \quad (7)$$

where $\epsilon_{ij} = \sqrt{\epsilon_i \epsilon_j}$ is the combined LJ well-depth for solute site i and solvent site j , r is the distance between site i and j , and $R_{ij}^* = (R_i^* + R_j^*)/2$ is the average of the minimum-energy distances of ii and jj type interactions. An elegant separation of repulsive and attractive forces in LJ potential was originally developed by WCA in the context of liquid perturbation theory.¹⁹ According to the WCA separation, the repulsive and attractive contribution to the LJ potential are

$$u_{ij}^{\text{rep}}(r) = \begin{cases} \epsilon_{ij} \left[\left(\frac{R_{ij}^*}{r} \right)^{12} - 2 \left(\frac{R_{ij}^*}{r} \right)^6 + 1 \right] & r \leq R_{ij}^* \\ 0 & r > R_{ij}^* \end{cases} \quad (8)$$

and

$$u_{ij}^{\text{dis}}(r) = \begin{cases} -\epsilon_{ij} & r \leq R_{ij}^* \\ \epsilon_{ij} \left[\left(\frac{R_{ij}^*}{r} \right)^{12} - 2 \left(\frac{R_{ij}^*}{r} \right)^6 \right] & r > R_{ij}^* \end{cases} \quad (9)$$

respectively. Accordingly, the total solute–solvent potential energy can be expressed as

$$U_{\text{uv}}^{\text{np}}(\mathbf{X}, \mathbf{Y}) = U_{\text{uv}}^{\text{rep}}(\mathbf{X}, \mathbf{Y}) + U_{\text{uv}}^{\text{dis}}(\mathbf{X}, \mathbf{Y}) \quad (10)$$

where $U_{\text{uv}}^{\text{rep}}(\mathbf{X}, \mathbf{Y})$ and $U_{\text{uv}}^{\text{dis}}(\mathbf{X}, \mathbf{Y})$ are the total solute–solvent LJ–WCA repulsion and dispersion interactions summed on solute–solvent sites. A decomposition of the nonpolar free energy ΔG^{np} follows from the WCA separation scheme

$$\Delta G^{\text{np}} = \Delta G^{\text{rep}} + \Delta G^{\text{dis}} \quad (11)$$

where

$$\Delta G^{\text{rep}} = -\frac{1}{\beta} \ln \left[\frac{\int d\mathbf{X} d\mathbf{Y} e^{-\beta[U_{\text{u}}(\mathbf{X}) + U_{\text{v}}(\mathbf{Y}) + U_{\text{uv}}^{\text{rep}}(\mathbf{X}, \mathbf{Y})]}}{\int d\mathbf{Y} e^{-\beta U_{\text{v}}(\mathbf{Y})} \int d\mathbf{X} e^{-\beta U_{\text{u}}(\mathbf{X})}} \right] \quad (12)$$

and

$$\Delta G^{\text{dis}} = -\frac{1}{\beta} \ln \left[\frac{\int d\mathbf{X} d\mathbf{Y} e^{-\beta[U_{\text{u}}(\mathbf{X}) + U_{\text{v}}(\mathbf{Y}) + U_{\text{uv}}^{\text{rep}}(\mathbf{X}, \mathbf{Y}) + U_{\text{uv}}^{\text{dis}}(\mathbf{X}, \mathbf{Y})]}}{\int d\mathbf{X} d\mathbf{Y} e^{-\beta[U_{\text{u}}(\mathbf{X}) + U_{\text{v}}(\mathbf{Y}) + U_{\text{uv}}^{\text{rep}}(\mathbf{X}, \mathbf{Y})]}} \right] \quad (13)$$

are the repulsive and dispersive free energy, respectively.

B. Thermodynamic Coupling Parameters. The three main contributions to the solvation free energy, ΔG^{rep} , ΔG^{dis} , and ΔG^{elec} , can be calculated with free energy perturbation techniques (FEP).^{23–25} For example, the free energy difference $[G_j - G_i]$ corresponding to a change in the potential energy, $U_i \rightarrow U_j$, can be calculated as an average over an ensemble of configurations generated with the potential energy U_i

$$[G_j - G_i] = -\frac{1}{\beta} \ln \left[\langle e^{-\beta[U_j - U_i]} \rangle_{(U_i)} \right] \quad (14)$$

where the angular brackets denote a configurational average in the canonical ensemble. However, this technique works in practice only if the change in the potential energy does not perturb the initial configuration space too abruptly. To compute free energy differences caused by a large perturbation, intermediate potential energy surfaces, $U(\lambda)$, are typically constructed by using a thermodynamic coupling parameter, λ with $0 \leq \lambda \leq 1$, such that $U(\lambda = 0) = U_i$ and $U(\lambda = 1) = U_j$. In principle, any arbitrary perturbation can be treated with the FEP by considering successive interval of the thermodynamic coupling parameter. When the perturbation involves a smoothly varying interaction, as with the solute–solvent electrostatic or dispersive interactions, a linear combination between the end states U_i and U_j , $U(\lambda) = (1 - \lambda)U_i + \lambda U_j$, is adequate. However, the calculation of ΔG^{rep} , corresponding to the reversible thermodynamic work done by the solute–solvent core repulsion interaction, requires special attention. A linear coupling scheme encounters problems such as “end-point catastrophe” and nonintegrability of the ensemble average²⁶ in free energy simulations because of the harsh nature of the repulsion potential. To avoid such problems, the repulsive part of the LJ–WCA potential is transformed into a soft-core potential con-

trolled by the nonlinear staging parameter s

$$u_{ij}^{\text{rep}}(r; s) = \begin{cases} \epsilon_{ij} \left\{ \frac{(R_{ij}^*)^{12}}{[r^2 + (1-s)(R_{ij}^*)^2]^6} - 2 \frac{(R_{ij}^*)^6}{[r^2 + (1-s)(R_{ij}^*)^2]^3} + 1 \right\} & r \leq R_{ij}^* \sqrt{1 - (1-s)^2} \\ 0 & r > R_{ij}^* \sqrt{1 - (1-s)^2} \end{cases} \quad (15)$$

When $s = 0$, $u_{ij}^{\text{rep}}(r, s) \equiv 0$, and when $s = 1$, the pair potential $u_{ij}^{\text{rep}}(r, s)$ is equivalent to the original WCA repulsive pair potential, $u_{ij}^{\text{rep}}(r)$. The way the stage parameter is introduced in eq 15 is similar to the separated shift parameter²⁷ and four-dimensional displacement²⁸ in existing literature.

To summarize, for the free energy simulation, the potential energy is expressed in terms of three coupling (staging) parameters s , ξ , and λ as

$$U(\mathbf{X}, \mathbf{Y}; s, \xi, \lambda) = U_{\text{u}}(\mathbf{X}) + U_{\text{v}}(\mathbf{Y}) + U_{\text{uv}}^{\text{rep}}(\mathbf{Y}, \mathbf{X}; s) + \xi U_{\text{uv}}^{\text{dis}}(\mathbf{Y}, \mathbf{X}) + \lambda U_{\text{uv}}^{\text{elec}}(\mathbf{Y}, \mathbf{X}) \quad (16)$$

where $U_{\text{uv}}^{\text{rep}}(\mathbf{Y}, \mathbf{X}; s)$ is the total shifted solute–solvent repulsion based on the shifted repulsive pair potential in eq 15. With this formulation, each component of the excess solvation free energy can be readily evaluated. The reversible work corresponding to the insertion of the fully interacting solute into the solvent can be done as follows: the solute–solvent core repulsion is progressively introduced in a first step

$$\Delta G^{\text{rep}} \equiv U(s = 0, \xi = 0, \lambda = 0) \rightarrow U(s = 1, \xi = 0, \lambda = 0) \quad (17)$$

the solute–solvent van der Waals dispersion is then introduced in the second step

$$\Delta G^{\text{dis}} \equiv U(s = 1, \xi = 0, \lambda = 0) \rightarrow U(s = 1, \xi = 1, \lambda = 0) \quad (18)$$

and the solute–solvent electrostatic interactions are finally introduced in the third and last step

$$\Delta G^{\text{elec}} \equiv U(s = 1, \xi = 1, \lambda = 0) \rightarrow U(s = 1, \xi = 1, \lambda = 1) \quad (19)$$

Finally, the total solvation free energy is the sum of the contributions from the three processes above: $\Delta G^{\text{tot}} = \Delta G^{\text{rep}} + \Delta G^{\text{dis}} + \Delta G^{\text{elec}}$.

C. Computational Details. The staged free energy simulation scheme, with the three coupling (staging) parameters, s , ξ , and λ , was implemented in the PERT module of the program CHARMM.²⁹ The free energy contribution from the core repulsion was calculated by setting the staging parameter s to 0.0, 0.2, 0.3, 0.4, 0.5, 0.6, 0.7, 0.8, 0.9, and 1.0. For each value of s , two trajectories of 30 ps were run for both the initial and final states. Only the last 20 ps of each trajectory was used in the free energy calculations. The free energy contribution from electrostatics and from the van der Waals dispersion interactions were both calculated using a standard linear coupling scheme. For the dispersive attraction, the coupling parameter ξ was set to 0.0, 0.1, 0.2, 0.3, 0.4, 0.5, 0.6, 0.7, 0.8, 0.9, and 1.0. For the electrostatic free energy contribution, the coupling parameter λ was set to 0.0, 0.1, 0.2, 0.3, 0.4, 0.5, 0.6, 0.7, 0.8, 0.9, and 1.0. In both cases, interaction energy samples were collected from the last 20 ps of two 30 ps trajectories and the samples were processed by the weighted histogram analysis method (WHAM).^{30–32} In practice, all nonbonded interactions involving

the solute (solute–solvent as well as solute–solute internal contributions) were modified by the coupling parameters s , ξ , and λ . Therefore, the free energies calculated in vacuo were subtracted from the value calculated in water to remove all internal energy contributions for each solute. The in vacuo free energies were calculated (without solvent molecules) using exactly the same coupling parameter schemes as in simulations with solvent.

The staged simulation protocol was first applied to the hydration of water, methane, benzene, and butane, and then to the hydration of protein amino acid side chains. The benzene molecule was represented by the all-atom model developed by Jorgensen and Severance,³³ whereas the methane and butane molecules were modeled according to the CHARMM PARAM22 force field.⁹ The all-atom CHARMM PARAM22⁹ and the AMBER¹⁰ force fields were used to represent the amino acid side chains. The TIP3P water model³⁴ was used for both solvent and solute water. Unless specified otherwise, all free energies were calculated with 100 explicit water molecules, with the influence of the remaining bulk being incorporated via the spherical solvent boundary potential (SSBP).¹⁸ The system temperature was held fixed at 300 K with Langevin dynamics. A friction constant of 5 ps⁻¹ was applied on the oxygen atoms of all of the water molecules. The integration time step of the dynamics was 2 fs. All bonds involving in the hydrogen atom were fixed with SHAKE constraints.³⁵ The center of mass of the solute was constrained to the center of the solvent sphere with a harmonic potential with a force constant of 1.0 kcal·Å⁻²·mol⁻¹.

SSBP is an approximation that aims at simulating the properties of an infinite bulk water system using a finite number of explicit water molecules in a spherical region centered around the mass center of the solute.¹⁸ The total potential energy of the system with SSBP is

$$W(\mathbf{X}, \mathbf{Y}) = U_{\text{u}}(\mathbf{X}) + U_{\text{v}}(\mathbf{Y}) + U_{\text{uv}}(\mathbf{Y}, \mathbf{X}) + \Delta W(\mathbf{X}, \mathbf{Y}) \quad (20)$$

where $\Delta W(\mathbf{X}, \mathbf{Y})$ is the solvent boundary potential. Previous experience showed that SSBP provides an accurate representation of the long-range electrostatic interactions with modest computational effort (although the results for charged species must be interpreted with care, see below).¹⁸ However, preliminary calculations with the staged free energy protocol indicated that the internal pressure is slightly overestimated in a finite-size spherical system because of the approximations used in the implementation of SSBP potential. As a result, the free energy contribution from the core repulsive interactions is typically overestimated in calculations based on the original implementation of SSBP if the number of explicit solvent molecule is not sufficiently large. The problem becomes negligible if a spherical system including a large number of explicit solvent molecules is used. However, a computational protocol able to yield accurate free energies from simulations including as small a number of solvent as possible is more advantageous. A simple empirical correction was introduced to correct this inadequacy

$$\Delta W^{\text{pres}} = \frac{p_1 R^0}{R_{\text{max}}} \sum_{i=1}^n e^{-p_2 R_i^2 / (R_{\text{max}} / R^0)^2} \quad (21)$$

where n is the number of water molecules, R_i is the distance from the oxygen of water molecule i to the center of the spherical simulation region, and R_{max} is the distance of the farthest water oxygen. By construction, the empirical correction

vanishes when the size of the system approaches infinity, i.e., a system with an infinite number of water molecules does not need the correction. Such a functional form of the empirical correction is not meant to be unique, e.g., the gyration-radius-based pressure constraint³⁶ could also be used. The quantities p_1 , p_2 , and R^0 are empirical parameters that were adjusted to reproduce the results from isobaric–isothermal MD simulations with periodic boundary conditions (PBC); p_1 determines the magnitude of the correction potential, whereas p_2 and R^0 control the effective range of the potential. Calculations based on a benzene model by Jorgensen and Severance³³ were used to calibrate the empirical pressure-correction to SSBP. The result with SSBP and 100 water molecules was made to match (within 0.5 kcal/mol) the results obtained from MD simulations of one benzene in 125 water molecules with PBC. The electrostatic interactions were calculated using the particle mesh Ewald summation; the Ewald coefficient was set to 0.34 Å⁻¹. A sixth-order B-spline interpolation was applied on a 32 × 32 × 32 grid. The pressure was held at 1.0 atm using the Langevin piston method³⁷ with a pressure piston mass of 400.0 amu and a piston collision frequency 20 ps⁻¹. Hoover thermostat³⁸ with a “mass” of 3000.0 kcal·ps² held the temperature at 300 K. The same coupling parameter scheme and simulation lengths were used in both the PBC and SSBP simulations. In the final empirical correction potential, ΔW^{pres} , R^0 was set to 8.88 Å, as it is the average sphere size for 100 water molecules. Trial and error showed that appropriate values for p_1 and p_2 were 1.1 kcal/mol and 0.008 Å⁻². With these optimal values, the empirical pressure-correction is very small, inducing no noticeable effects in the liquid structure around the solute.

In the original SSBP implementation, the van der Waals dispersive interactions between the solute and the implicit solvent region were not included. Although the dispersive interaction decays rapidly, as $1/r^6$, the free energy contribution from the solvent molecules that are located beyond the radius of the spherical simulation region (typically 8–12 Å) is not completely negligible. Assuming that the solvent density is uniform beyond the finite simulation system, the contribution from the dispersive interaction can be easily taken into account by a long-range correction

$$\begin{aligned} \Delta G^{\text{Lrc}} &= \sum_{i \in \text{solute}} \sum_{j \in \text{solvent}} \epsilon_{ij} \rho_w \int_{r_c}^{\infty} 4\pi r^2 \left[\left(\frac{R_{ij}^*}{r} \right)^{12} - 2 \left(\frac{R_{ij}^*}{r} \right)^6 \right] dr \\ &\approx - \frac{8\pi \rho_w}{3r_c^3} \sum_{i \in \text{solute}} \sum_{j \in \text{solvent}} \epsilon_{ij} (R_{ij}^*)^6 \end{aligned} \quad (22)$$

where ρ_w is the number density of bulk water and r_c is the average radius of the spherical region of explicit water molecules.

The electrostatic free energy contribution for solutes carrying a net charge must be interpreted with care. In a real physical system, the total free energy should include a contribution from the electrostatic potential associated with the liquid–vapor interface. Such electrostatic potential arises from the anisotropic orientational distribution of the solvent molecules near the interface. Although the interfacial potential is difficult to measure experimentally, estimates from computer simulations indicate that it is roughly +450 mV for liquid water relative to vapor.³⁹ The existence of the interfacial potential implies that there is an offset contribution of about –10 kcal/mol for the electrostatic free energy of a monovalent cation and about +10 kcal/mol for the electrostatic free energy of a monovalent anion;

TABLE 1: Excess Hydration Free Energies of Water, Methane, Benzene, and Butane with Their Experimental Counterparts^a

	ΔG^{rep}		ΔG^{dis}		ΔG^{np}		ΔG^{lrc}		ΔG^{elec}		ΔG^{total}		$\Delta G^{\text{exp } b}$
	SSBP	PBC	SSBP	PBC	SSBP	PBC	SSBP	PBC	SSBP	PBC	SSBP	PBC	
water	5.26	4.98	-2.74	-2.65	2.52	2.33	-0.12	0.00	-8.12	-8.26	-5.72	-5.93	-6.31
methane	5.98	6.31	-4.01	-4.11	1.97	2.20	-0.14	0.00	-0.03	-0.03	1.80	2.17	2.00
benzene	14.36	13.30	-11.96	-11.47	2.40	1.83	-0.70	0.00	-2.02	-1.83	-0.31	0.00	-0.87
butane	14.17	12.79	-10.77	-10.25	3.40	2.54	-0.55	0.00	-0.15	-0.12	2.70	2.42	2.08

^a TIP3P water model is used as solute water. Benzene model is the slightly modified one in CHARMM PARAM22 force field⁹ derived from the work of Jorgensen and Severance.³³ Methane and butane molecules are modeled according to the CHARMM PARAM22 force field. 100 and 125 TIP3P water molecules are used in the SSBP and PBC calculations, respectively. The repulsive and dispersive as well as the electrostatic contribution of the free energies are also given. The nonpolar free energy is a sum of the repulsive and dispersive free energies from free energy perturbation. The total is the sum of repulsive, dispersive, electrostatic, and long-range contribution. All of the free energy values are in kcal·mol⁻¹. ^b From ref 50.

as expected, the energy offsets cancel out if a cation and an anion are dissolved simultaneously. The contribution of the interfacial potential should be included in the calculated free energy for meaningful comparison with experiments. Remarkably, a potential difference with a similar magnitude is induced at the edge of the finite simulation system in SSBP calculations, where the explicit water molecules are near the smooth dielectric boundary of the system (Lamoureux and Roux, in preparation). Therefore, the interfacial potential contribution is effectively included in SSBP calculations. In contrast, it is formally excluded in free energy calculations based on PME with PBC because there is no physical interface.⁴⁰

III. Results and Discussion

A. Solvation Free Energy of Water, Methane, Benzene and Butane. The complete staged simulation protocol, including the nonpolar and electrostatic contribution, was first applied to the hydration of water, methane, benzene, and butane. The calculated free energy values are listed in Table 1. As with previous simulation results,^{15,41} the computed free energies tend to be slightly larger than the experimental values. Nonetheless, the overall agreement is reasonable, considering the statistical uncertainty of the computed free energies.

The progressive transformation of the LJ-WCA repulsion and dispersion potential with respect to the coupling (staging) parameters s and ξ is shown in Figure 1 for the TIP3P oxygen–oxygen interaction. The solute–solvent repulsion increases gradually from $s = 0$ to 1. Such transformation of the repulsive potential with nonlinear scaling shown in eq 15 is similar in spirit to other approaches commonly used in free energy computations, e.g., the soft-core potential,⁴² the separation-shifted scaling,²⁷ and the dynamical displacements in four dimensional space.²⁸ Shown also in Figure 1 is the coupling of the dispersion interaction with the parameter ξ . The linear coupling scheme smoothly turns on the attractive LJ well from $\xi = 0$ to 1. Describing the nonpolar free energy calculation in terms of an insertion process (though a deletion process would be equivalent), the increase in the nonlinear coupling carries on the insertion process gradually. Consequently the difficulties encountered by Widom insertion at high density⁴³ are overcome by progressive staging via the nonlinear coupling parameter s introduced in the WCA repulsive potential. A smooth transition from noninteracting solute to weakly interacting solute is guaranteed in the first step of the perturbation (when the coupling parameter goes from $s = 0 \rightarrow s = 0.2$) because the repulsion at zero distance corresponds to an energy which is only on the order of $k_B T$. The catastrophic “end-point” singularity²⁶ caused by the harsh repulsive potential is thus avoided completely.

In the insertion process, the repulsion must be introduced first to create a cavity in the liquid, and only then, the remaining

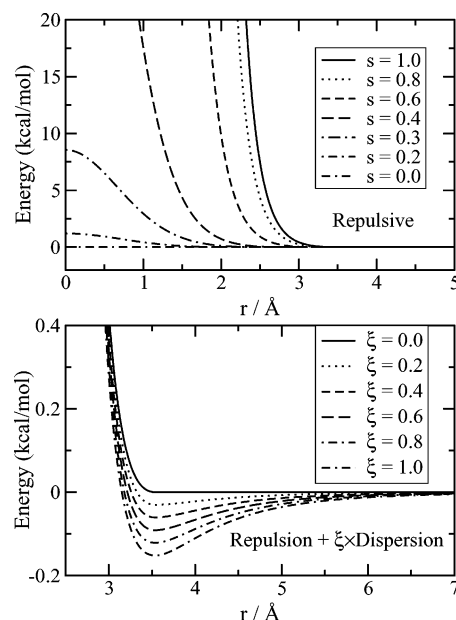


Figure 1. Staged TIP3P oxygen–oxygen LJ interaction. Plotted in the upper panel is the WCA repulsive potential between two TIP3P oxygen atoms at various values of parameter, s . In the lower panel is sum of the WCA repulsive and linearly scaled (by ξ) dispersive potential. $R_0^* = 3.536$ Å, and $\epsilon_0 = 0.152$ kcal/mol.³⁴

attractive contributions (dispersion or electrostatics) can be added. In the current work, the dispersion was introduced before electrostatics to group together all the nonpolar contributions. The complete free energy progression of water as a function of all the coupling parameters s , ξ and λ is shown in Figure 2. The electrostatic free energy shows the typical linear parabolic behavior with respect to the electrostatic coupling parameter λ (e.g., see ref 44). Since electrostatics makes a small contribution to the hydration free energy of hydrophobic molecules, only the repulsion–dispersion free energies as a function of the coupling parameters are shown in Figures 3–5, for methane, benzene, and butane, respectively. For all of these molecules, there is a monotonic progression of the free energy through intermediate simulation states. In comparison, the repulsive free energy does not behave as smoothly with respect to the staging parameter s . There is an apparent cusp around $s = 0.2$ (mostly apparent for benzene). However, this does not present any problem to the free energy computation with FEP, which does not require the derivative of the free energy to be smoothly continuous with respect to the coupling (staging) parameter.

All of the free energies given in Table 1 were obtained with 100 explicit solvent water molecules. It has been previously shown that the electrostatic contribution is weakly sensitive to the number of water molecules.¹⁸ However, the computed values

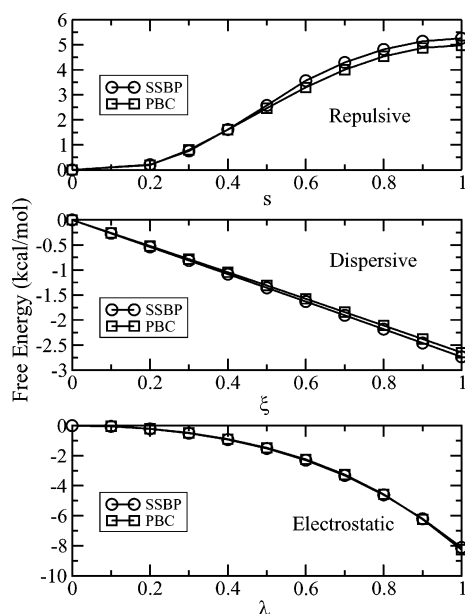


Figure 2. Excess free energy of water hydration. Shown in the top panel is the nine-stage free energy progression of the repulsive free energy. The middle panel shows the dispersive free energy progression as a function of coupling parameter, ξ . The bottom panel shows the charging of an uncharged water molecule as a function of the coupling parameter, λ . The results of both constant temperature and pressure molecular dynamics with periodic boundary condition (PBC) and SSBP are plotted for comparison. 100 water molecules are used as solvent.

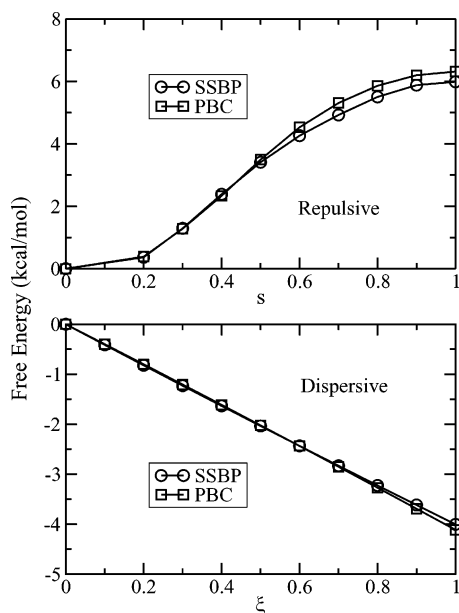


Figure 3. Excess free energy of methane hydration. Shown in the top panel is the nine-stage free energy progression of the repulsive free energy as a function of the parameter, s . The bottom panel shows the dispersive free energy progression as a function of the coupling parameter, ξ . The results of both constant temperature and pressure molecular dynamics with periodic boundary condition (PBC) and SSBP are plotted for comparison. 100 water molecules are used as solvent.

of the nonpolar contributions could be affected by the number of water molecules included explicitly. In its original implementation,¹⁸ SSBP does not include the van der Waals interactions of the solute with the solvent molecules located in the “outer region”, which is not represented explicitly. As a consequence, a significant fraction of the favorable solvation free energy is not included in the calculation when the simulated spherical system is relatively small. As seen in Table 1, the

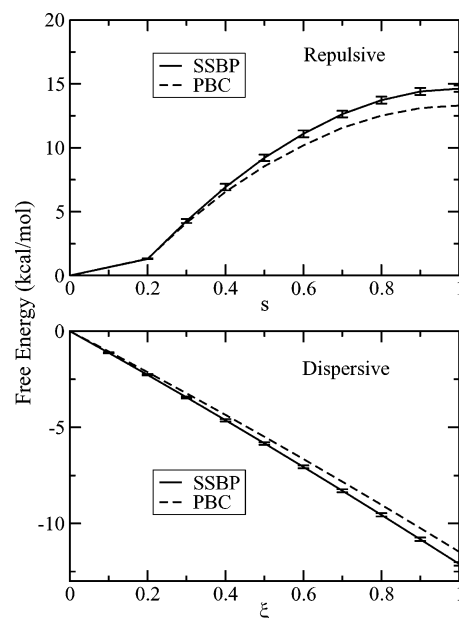


Figure 4. Excess free energy of uncharged benzene hydration. Shown in the top panel is the nine-stage free energy progression of the repulsive free energy as a function of the parameter s . The bottom panel shows the dispersive free energy progression as a function of the coupling parameter ξ . The results of both constant temperature and pressure molecular dynamics with periodic boundary condition (PBC) and SSBP are plotted for comparison. The errors are computed as the standard deviation from 10 simulations with different initial velocities. 100 water molecules are used as solvent.

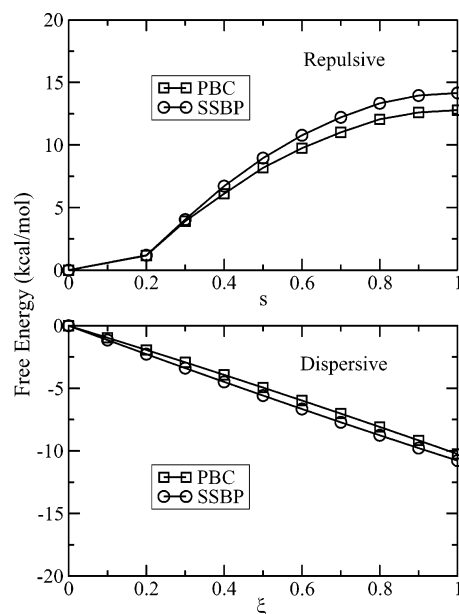


Figure 5. Excess free energy of uncharged butane hydration. Shown in the top panel is the nine-stage free energy progression of the repulsive free energy as a function of the parameter s . The bottom panel shows the dispersive free energy progression as a function of the coupling parameter ξ . The results of both constant temperature and pressure molecular dynamics with periodic boundary condition (PBC) and SSBP are plotted for comparison. One hundred explicit water molecules are used in the SSBP calculation.

results from SSBP tend to be greater than those of PBC if such favorable contribution is neglected. However, the SSBP nonpolar free energy becomes closer to the PBC values (except for methane) once a long-range correction based on eq 22 is included. To further assess the effect of the number of explicit water molecules on the accuracy of the results from SSBP, the

TABLE 2: Nonpolar Free Energies of Benzene Hydration Computed in 25, 50, 100, 200, and 400 TIP3P Water Molecules with SSBP^a

number of water	400	200	100	50	25
ΔG^{rep}	15.07	15.22	14.36	10.64	9.20
ΔG^{dis}	-13.09	-12.78	-11.96	-7.44	-5.37
ΔG^{lrc}	-0.17	-0.34	-0.70	-1.19	-2.36
$\Delta G^{\text{dis}} + \Delta G^{\text{lrc}}$	-13.26	-13.12	-12.66	-8.63	-7.73
$\Delta G^{\text{rep}} + \Delta G^{\text{dis}} + \Delta G^{\text{lrc}}$	1.81	2.10	1.70	2.01	1.47

^a The long-range correction for the SSBP systems of 25, 50, 100, 200, and 400 water molecules used eq 22 with spherical radii of 5.9, 7.43, 8.88, 11.28, and 14.10 Å, respectively. The nonpolar free energy is a sum of the repulsive and dispersive free energies from free energy perturbation. All of the free energy values are in kcal·mol⁻¹.

nonpolar free energy of benzene was recalculated using 25, 50, 200, and 400 water molecules. The results with different number of water molecules are listed in Table 2. The repulsion free energy converges to a stable value of about +14.5 to +15.0 kcal/mol with more than 100 explicit water molecules. The total dispersive free energy (including the long-range correction) also converges to a stable value of about -12.5 to -13.5 kcal/mol, though the uncertainty seem to be slightly larger in this case. Part of the variations may be due to the finite size of the benzene molecule compared to the radius of the simulated SSBP system, which is ignored in the long-range correction based on eq 22. The total nonpolar free energy ($\Delta G^{\text{rep}} + \Delta G^{\text{dis}} + \Delta G^{\text{lrc}}$) is remarkably similar, although the individual contributions from repulsion and attraction display significant variations in the different systems ranging from 25 to 400 water molecules. The apparent convergence of $\Delta G^{\text{rep}} + \Delta G^{\text{dis}} + \Delta G^{\text{lrc}}$ with 25 and 50 water molecules is partly due to the cancellation of error in the repulsive and attractive contributions. It is likely that results obtained with 100 or more water molecules are going to be more reliable than those from 25 and 50 water molecules, as indicated by the convergence of the individual components. Weighing computational effort and accuracy, we used 100 TIP3P water molecules as solvent, throughout the rest of this paper. Since the long-range correction based on eq 22 always improves the results, it is always included in the total excess solvation free energy.

To assess the statistical precision of the calculated free energy, we repeated the free energy calculation for benzene in 100 explicit water molecules for 10 simulations generated from different initial velocities. The standard deviations of the repulsive, dispersive, and electrostatic free energies are 0.26, 0.09, and 0.05 kcal/mol, respectively. The precision of our results is indeed less than the 0.02–0.05 kcal/mol uncertainty of Shirts et al.¹⁵ However, in the work of Shirts et al., the simulation length was 1.2 ns per sampling window and 61 windows (λ values), whereas it is only 40 ps and 40 windows in the present computations (sum of number of λ , ξ , and twice the number of s values). The larger uncertainty seems well-justified, given that the present effort represents only two percent of the computations of Shirts et al.¹⁵ Furthermore, the uncertainty is comparable to previous results from thermodynamic integration (TI) calculations (which required more sampling).^{41,45,46} One feature of the error bars displayed Figure 4 is that the statistical uncertainty appears to be of similar magnitude along the repulsive and dispersive free energy simulation paths, respectively. In contrast, the behavior appears to be different when the standard LJ potential (including both repulsion and attraction) is introduced all at once. In TI calculations for example, the fluctuations of the integrand are largest near the middle of the simulation path between the two end-points.^{15,26} Therefore,

the WCA decomposition of the LJ potential may actually help improve the sampling efficiency in free energy simulations.

It is apparent, from Figures 2–4, that the progression of the dispersion free energy contribution with respect to the coupling parameter ξ is nearly linear, suggesting that a smaller number of intermediate values of ξ would be adequate. This near-linear free energy progression is indeed a confirmation of the original van der Waals picture that dispersion effects can be treated perturbatively.⁴⁷ As a test, we reduced the number of ξ values to six (i.e., 0.0, 0.2, 0.4, 0.6, 0.8, and 1.0) and used only half the samples for benzene dispersive free energy. The resulting dispersive free energy ends up being -12.10 kcal/mol (-11.96 kcal/mol is the original) and a standard deviation of 0.15 kcal/mol calculated from 10 different simulations launched from different initial velocities. With about one-fourth of sampling, there is only 0.06 kcal/mol increase in the uncertainty. This test confirms that the dispersion free energy does not really require extensive sampling. Nonetheless, we used 11 ξ values to compute the free energy contribution from the dispersive interaction energy throughout the remainder of this paper for the sake of consistency.

The total nonpolar free energies of water, methane, benzene, and butane is around 2–3 kcal/mol. Nonetheless, it should be emphasized that such small values hide the significantly larger repulsive and dispersive free energy contributions, which nearly cancel one another.^{21,22} Those individual contributions have opposite sign. With WCA, the reversible work for cavity formation yields a positive-definite free energy contribution, i.e., $\Delta G^{\text{rep}} \geq 0$. The attractive dispersion on the other hand yields a negative contribution, i.e., the dispersion enhances the affinity of the solute and solvents and $\Delta G^{\text{dis}} \leq 0$. In Table 1, such a trend is evident. By design of the WCA decomposition, both contributions are as small as possible.⁴⁷ The near-cancellation may, in part, explain how introducing the repulsive and attractive parts of the potential simultaneously with a single thermodynamic coupling parameter could give rise to a nonmonotonic progression of the free energy as observed by Zacharias et al.²⁷ or Pomès et al.²⁸ One may note that, although the large contributions of the repulsive and attractive part of the potential to the hydration free energy nearly cancel one another, such a balance could be very different in environments other than liquid water. Variations in the local surrounding of a solute could have a significant impact on the nonpolar free energy. For example, a cavity of a given size might be preformed in the interior of a protein, causing a significant reduction in the reversible work needed for insertion of the solute. Furthermore, the atomic density is much higher inside a protein than in liquid water, increasing the magnitude of the favorable free energy contribution from van der Waals dispersion. Such observations might be helpful to improve current implicit solvent models to use in protein–ligand binding and to better understand the factors governing hydrophobic solvation and protein stability.^{12,17}

B. Free Energies of Amino Acid Side Chains. The hydration of amino acid side chains is of fundamental importance for the stability of proteins.^{45,46,48} The calculation of the side chain hydration free energies of 18 of the 20 naturally occurring amino acids (glycine and proline excluded) is thus chosen to test the staged free energy simulation protocol further. The side chain models are generated from amino acid residues by the substitution of the α carbon with a hydrogen atom and partial charge adjustment on the β carbon to preserve electroneutrality.¹⁵ The hydration free energies were computed using both the CHARMM PARAM22⁹ and the AMBER¹⁰ side chain models. The results

TABLE 3: Excess Free Energy Values of Amino Acid Side Chains Computed with the CHARMM PARAM22 Force Field^a

molecule	residue	ΔG^{rep}	ΔG^{dis}	ΔG^{np}	ΔG^{lrc}	ΔG^{elec}	ΔG^{total}	$\Delta G^{\text{exp } b}$
<i>n</i> -butane	Ile	14.17	-10.77	3.40	-0.55	-0.15	2.70	2.08
isobutane	Leu	13.45	-10.04	3.41	-0.51	-0.10	2.80	2.28
methane	Ala	5.98	-4.01	1.97	-0.14	0.03	1.86	2.00
propane	Val	12.19	-8.88	3.31	-0.41	-0.07	2.83	1.96
acetamide	Asn	11.74	-9.09	2.65	-0.51	-9.26	-7.12	-9.72
<i>p</i> -cresol	Tyr	17.64	-14.75	2.89	-0.96	-6.01	-4.08	-6.13
ethanol	Thr	10.94	-8.13	2.81	-0.40	-6.49	-4.08	-4.90
methanethiol	Cys	9.61	-8.23	1.38	-0.44	-1.16	-0.22	-1.24
methanol	Ser	8.35	-5.90	2.45	-0.26	-7.07	-4.88	-5.08
methylethyl sulfide	Met	14.47	-12.22	2.25	-0.71	-0.60	0.93	-1.49
3-methylindole	Trp	19.83	-16.82	3.01	-1.19	-4.73	-2.91	-5.91
methylimidazole ^c	Hid	14.05	-11.45	2.60	-0.67	-11.42	-9.49	-10.25
methylimidazole ^d	Hie	13.43	-11.34	2.09	-0.67	-11.67	-10.25	-10.25
propionamide	Gln	13.86	-10.98	2.88	-0.64	-9.08	-6.84	-9.42
toluene	Phe	16.93	-13.76	3.17	-0.84	-1.67	0.66	-0.76
acetate	Asp	10.73	-8.22	2.51	-0.44	-82.69	-80.62	-80.65
<i>n</i> -butylammonium	Lys	15.77	-12.44	3.33	-0.71	-67.51	-64.89	-69.24
<i>n</i> -propylguanidinium	Arg	17.30	-15.27	1.73	-1.03	-60.14	-59.44	
propionate	Glu	13.17	-10.29	2.88	-0.58	-82.84	-80.54	-79.12

^a The nonpolar free energy is a sum of the repulsive and dispersive free energies from free energy perturbation. The total is the sum of repulsive, dispersive, electrostatic, and long-range contribution. 100 water molecules are used as solvent. All of the free energy values are in kcal·mol⁻¹. ^b The free energy values of butane, methane and propane are taken from ref 50. The rest are taken from ref 16. ^c Hydrogen atom on δ nitrogen. ^d Hydrogen atom on ϵ nitrogen.

TABLE 4: Excess Free Energy Values of Amino Acid Side Chains Computed with AMBER Force Field^a

molecule	residue	ΔG^{rep}	ΔG^{dis}	ΔG^{np}	ΔG^{lrc}	ΔG^{elec}	ΔG^{total}	$\Delta G^{\text{exp } b}$
<i>n</i> -butane	Ile	14.68	-10.97	3.71	-0.51	-0.01	3.19	2.08
isobutane	Leu	14.76	-10.76	4.00	-0.51	-0.12	3.37	2.28
methane	Ala	7.37	-4.32	3.05	-0.13	-0.00	2.94	2.00
propane	Val	12.62	-8.97	3.65	-0.38	-0.05	3.22	1.96
acetamide	Asn	11.85	-9.51	2.34	-0.49	-10.32	-8.47	-9.72
<i>p</i> -cresol	Tyr	17.91	-14.60	3.31	-0.93	-6.32	-3.94	-6.13
ethanol	Thr	10.65	-8.33	2.32	-0.38	-5.72	-3.78	-4.90
methanethiol	Cys	9.68	-6.89	2.79	-0.35	-2.02	0.42	-1.24
methanol	Ser	8.57	-6.00	2.57	-0.26	-5.90	-3.59	-5.08
methylethyl sulfide	Met	14.73	-11.13	3.60	-0.60	-1.53	1.47	-1.49
3-methylindole	Trp	19.51	-16.41	3.10	-1.17	-5.06	-3.13	-5.91
methylimidazole ^c	Hid	14.35	-12.25	2.10	-0.74	-9.16	-7.80	-10.25
methylimidazole ^d	Hie	15.00	-12.60	2.40	-0.74	-9.83	-8.17	-10.25
propionamide	Gln	13.67	-11.42	2.25	-0.62	-10.95	-9.32	-9.42
toluene	Phe	16.73	-13.32	3.41	-0.80	-2.49	0.12	-0.76
acetate	Asp	11.09	-9.19	1.90	-0.47	-76.79	-75.36	-80.65
<i>n</i> -butylammonium	Lys	16.28	-12.54	3.74	-0.65	-57.30	-54.21	-69.24
<i>n</i> -propylguanidinium	Arg	17.77	-15.20	2.57	-0.91	-57.64	-55.98	
propionate	Glu	13.26	-10.96	2.30	-0.60	-71.07	-69.37	-79.12

^a The nonpolar free energy is a sum of the repulsive and dispersive free energies from free energy perturbation. The total is the sum of repulsive, dispersive, electrostatic, and long-range contribution. 100 water molecules are used as solvent. All of the free energy values are in kcal·mol⁻¹. ^b The free energy values of butane, methane and propane are taken from ref 50. The rest are taken from ref 16. ^c Hydrogen atom on δ nitrogen. ^d Hydrogen atom on ϵ nitrogen.

of the calculations for the CHARMM PARAM22 and AMBER amino acid side chain models are given in Tables 3 and 4, respectively.

The free energy values for the CHARMM PARAM22 and AMBER models are quite similar. In general, the results from both of these force fields agree with experimental values reasonably well, although all of the hydration free energies appear to be slightly less favorable than experimental values. The overestimation appears to be a common outcome of nonpolarizable atomic force fields.^{15,41} For charged side chains, the values from the AMBER force field deviates slightly more from the experimental values than those from CHARMM. It should be stressed, however, that the general agreement actually indicates the excellent performance of the CHARMM and AMBER potential functions since they were not originally optimized to reproduce experimental solvation free energies.^{9,10}

Recently Shirts et al.¹⁵ reported the results of extensive FEP calculations of the hydration free energy of amino acid side

chains for all three of the CHARMM PARAM22,⁹ AMBER,¹⁰ and OPLS-AA¹¹ force fields. Those calculations were generated through the usage of a large number of computers distributed around the world via the folding@home project. As those free energy calculations correspond to the highest precision ever achieved at the present time, they provide an excellent benchmark to assess the current protocol. For the CHARMM PARAM22 force field, the current results come to within 0.8 kcal/mol of those of Shirts et al.¹⁵ In the case of the AMBER force field, the current results agree with those of Shirts et al.¹⁵ with a maximum variation of 0.8 kcal/mol (with the exception of 3-methylindole and propionamide). Assuming that the overall statistical precision is similar to that of benzene (0.3 kcal/mol), such 0.8 kcal/mol maximum deviation shows excellent agreement between the current results and those of Shirts et al. The results are compared directly in Figures 6 and 7. For most of the side chains, the sub kilocalorie difference between the current results and those of Shirts et al.¹⁵ arises mainly from the

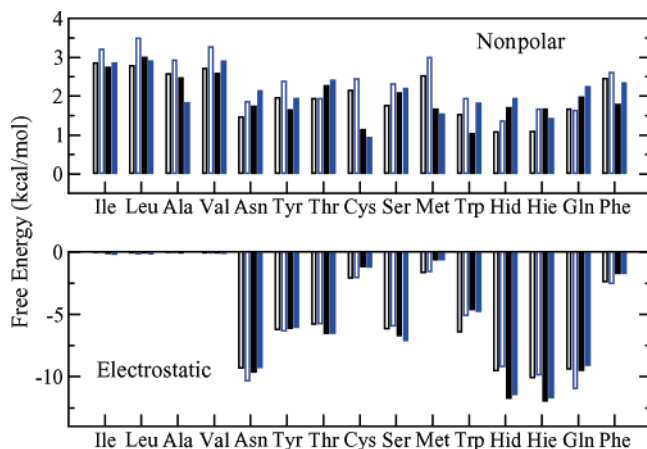


Figure 6. Nonpolar and electrostatic contribution to the solvation free energy of amino acid side chains for the CHARMM (filled bars) and AMBER (empty bars) force field from the present work (blue) and the calculation of Shirts et al. (black). Long-range correction is included in the nonpolar free energy.

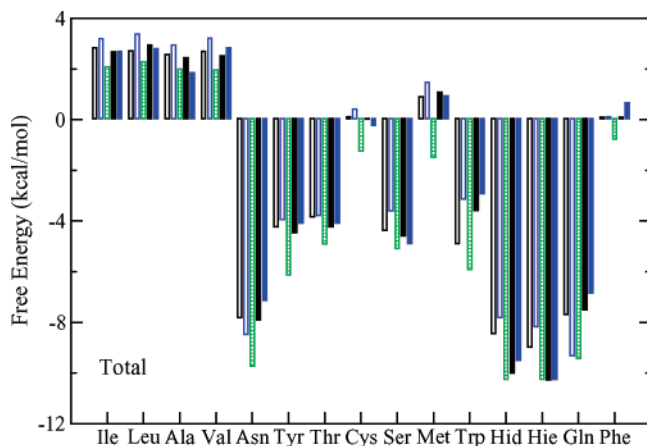


Figure 7. Total excess free energy of amino acid side chains for the CHARMM (filled bars) and AMBER (empty bars) force field from the present work (blue), the calculation of Shirts et al. (black), and experimental values (green).

nonpolar contribution. Exceptionally, the deviations with the results of Shirts et al. with the AMBER force field are 1.75 and -1.63 kcal/mol for 3-methylindole and propionamide, respectively. In these cases, the difference arises from the electrostatic contribution. Differences in simulation methodology and in the treatment of electrostatics might be the cause of such discrepancies. The simulations of Shirts et al.¹⁵ were carried out with PBC and a truncation scheme using a tapered coulomb potential. In contrast, all long-range electrostatic interactions are included in SSBP with no truncation in the current calculations. Charging free energy contributions calculated with SSBP simulations, which includes a solvent reaction field in the form of a Kirkwood multipolar expansion, has been shown previously to be fairly insensitive to the radius of the spherical region of explicit solvent.¹⁸

The calculated hydration free energies provide one important constraint on the atomic partial charge distribution in biomolecular force fields. An examination of the dipole moment for CHARMM PARAM22 models of some compounds indicates that there is significant difference between the one computed with the force field and the literature values. For example, the gas-phase dipole moment of methylethyl sulfide is about 1.6 D,⁴⁹ but only about 1.1 D from the CHARMM PARAM22 force field. In Table 5, we show that by increasing the dipole moment

TABLE 5: Electrostatic Free Energies of Methylethyl Sulfide with Different Partial Charges^a

methylethyl sulfide	
dipole	ΔG^{elec}
1.07 ^b	-0.60
2.81 ^c	-3.83

^a 100 water molecules are used as solvent. The unit of the free energies is kcal/mol, and the unit of dipole moment is debye.

^b CHARMM PARAM22 force field charges: S ^{δ} , $-0.09e$; C ^{γ} , $-0.14e$; C ^{ϵ} , $-0.22e$.

^c Charges: S ^{δ} , $-0.41e$; C ^{γ} , $0.02e$; C ^{ϵ} , $-0.06e$.

of methylethyl sulfide, the electrostatic free energy decreases; thus, the total free energies matches the experimental values much better. Ironically, even though the total dipole moment of the AMBER model of methylethyl sulfide is close to the literature value, the free energy value is not much improved compared with CHARMM PARAM22 force field. This suggests that the local charge distribution is also important in determining the solvation free energy. In the modified CHARMM methylethyl sulfide model, the charges on sulfur and its neighbor carbon atoms are quite close to those in the OPLS-AA¹¹ force field, which has been refined to reproduce hydration free energies. Indeed, the hydration free energy of methylethyl sulfide reported by Shirts et al.¹⁵ using OPLS-AA compared favorably with experiment than CHARMM PARAM22 and AMBER values. Clearly, other factors must also be taken into considerations to determine an optimal parametrization of the amino acid side chains. Nonetheless, since hydration free energy can be obtained relatively fast with the current protocol, it can be hoped that it will become a useful tool for refining biomolecular force fields.

IV. Conclusion

In this paper, we presented a staged simulation protocol for hydration free energy calculations. The free energy is divided into nonpolar and electrostatic contributions. The nonpolar contributions from the LJ potential, in turn, is separated into a repulsive and a dispersive part using the WCA scheme. The repulsive free energy is calculated in stages using a nonlinear coupling scheme via a soft-core transformation of the repulsive pair potential. The dispersive and electrostatic free energies are calculated with a linear coupling scheme. To reduce the computational effort, the free energy simulations are generated with a small number of explicit solvent water molecules near the solute of interest, whereas the influence of the remain bulk solvent is represented in terms of an effective solvent boundary potential. The latter approximation is, of course, independent of the staged free energy protocol which could be used as well with the computationally more expensive PBC simulations.

The nonlinear stages of the repulsive free energy successfully convert the particle insertion process to a progressive one, so that FEP can be used for each of the stages. The dispersion free energy progresses nearly linearly with respect to the coupling parameter, ξ . This confirms that the van der Waals picture of solvation is accurate and points out headroom for optimization. Indeed, a 70% reduction of the sampling gives virtually the same dispersion free energy and similar uncertainty. Test simulations show variations smaller than 0.5 kcal/mol for repulsive, dispersive, and electrostatic free energies with relatively modest computational effort. Further tests of the simulation protocol with amino acid-side-chain hydration free energy calculation for both CHARMM PARAM22 and AMBER force fields show reasonable agreement with experimental values and the high precision results of Shirts et al.¹⁵ The maximum

deviation of 0.8 kcal/mol from Shirts et al. for all CHARMM PARAM22 models and most of AMBER models demonstrates that the current simulation protocol is able to efficiently sample the configuration space and compute free energies accurately with modest effort.

In the development of FEP computational methodologies, issues of accuracy and precision are somewhat inter-related. The present FEP simulation protocol based on SSBP is "accurate" in the sense that the results are in good agreement with the calculations of Shirts et al.¹⁵ (the difference is less than 0.8 kcal/mol). Those calculations were based on extensive simulations with PBC, which is arguably more realistic than SSBP (though electrostatics was truncated). Using the current protocol with SSBP, one can achieve a statistical "precision" of less than 0.5 kcal/mol in FEP computations with relatively modest computational efforts. It is straightforward to improve the precision of such FEP calculations by increasing the simulation time. However, the true usefulness of FEP calculations is ultimately limited by the correctness of the nonpolarizable all-atom force field (CHARMM, AMBER, or OPLS). The calculations showed that the CHARMM and AMBER force fields reproduce experimental solvation free energies of amino acid side chains very well, though there is definitely room for improvement. From this point of view, the current protocol may become a useful tool for refining force fields by enabling rapid and inexpensive FEP calculations.

It is our hope that the current strategy will be useful for calculating the solvation free energy of small molecules with explicit solvent simulations in a computationally efficient way. Given the encouraging results, we will further develop this strategy for protein–ligand binding free energy calculations.

Acknowledgment. The authors are grateful to Guillaume Lamoureux, Toby Allen, Nilesh K. Banavali, Ken Dill, Vijay Pande, and Michael Shirts for helpful discussions. This work was supported by the National Science Foundation through Grant No. 0110847.

References and Notes

- Brooks, C., III; Karplus, M.; Pettitt, B. Proteins. A theoretical perspective of dynamics, structure and thermodynamics. In *Advances in Chemical Physics Vol. LXXI*; Prigogine, I., Rice, S. A., Eds.; John Wiley & Sons: New York, 1988.
- Karplus, M. *Acc. Chem. Res.* **2002**, *35*, 321–323.
- Vindigni, A. *Comb. Chem. High Throughput Screen.* **1999**, *2*, 139–153.
- Cheng, A. C.; Calabro, V.; Frankel, A. D. *Curr. Opin. Struct. Biol.* **2001**, *11* (4), 478–484.
- Garvie, C. W.; Wolberger, C. *Mol. Cell.* **2001**, *8* (5), 937–946.
- Smith, P. E.; Pettitt, B. M. *J. Phys. Chem.* **1994**, *98*, 9700–9711.
- Orozco, M.; Luque, F. J. *Chem. Rev.* **2000**, *100*, 4187–4225.
- Margenau, H. *Rev. Mod. Phys.* **1939**, *11*, 1–35.
- MacKerell, A. D., Jr.; et al. *J. Phys. Chem. B* **1998**, *102*, 3586–3616.
- Cornell, W. D.; Cieplak, P.; Bayly, C. L.; Gould, I. R.; Merz, K. M., Jr.; Ferguson, D. M.; Spellmeyer, D. C.; Fox, T.; Caldwell, J. W.; Kollman, P. A. *J. Am. Chem. Soc.* **1995**, *117*, 5179–5197.
- Jorgensen, W. L.; Maxwell, D. S.; Tirado-Rives, J. *J. Am. Chem. Soc.* **1996**, *118*, 11225–11236.
- Levy, R. M.; Zhang, L. Y.; Gallicchio, E.; Felts, A. K. *J. Am. Chem. Soc.* **2003**, *125*, 9523–9530.
- Boresch, S.; Archontis, G.; M. Karplus, *Proteins* **1994**, *20*, 25–33.
- Roux, B.; Simonson, T. *Biophys. Chem.* **1999**, *78*, 1–20.
- Shirts, M. R.; Pitera, J. W.; Swope, W. C.; Pande, V. S. *J. Chem. Phys.* **2003**, *119*, 5740–5761.
- Sitkoff, D.; Sharp, K. A.; Honig, B. *J. Phys. Chem.* **1994**, *98*, 1978–1988.
- Gallicchio, E.; Zhang, L. Y.; Levy, R. M. *J. Comput. Chem.* **2002**, *23*, 517–529.
- Beglov, D.; Roux, B. *J. Chem. Phys.* **1994**, *100*, 9050–9063.
- Weeks, J. D.; Chandler, D.; Andersen, H. C. *J. Chem. Phys.* **1971**, *54*, 5237–5247.
- Ding, K.; Valleau, J. P. *J. Chem. Phys.* **1993**, *98*, 3306–3312.
- Wescott, J. T.; Fisher, L. R.; Hanna, S. *J. Chem. Phys.* **2002**, *116*, 2361–2369.
- Straatsma, T. P.; Berendsen, H. J. C.; Postma, J. P. M. *J. Chem. Phys.* **1986**, *85*, 6720–6727.
- Zwanzig, R. *J. Chem. Phys.* **1954**, *22*, 1420–1426.
- Kollman, P. *Chem. Rev.* **1993**, *93*, 2395–2417.
- Straatsma, T. P.; McCammon, J. A. *Annu. Rev. Phys. Chem.* **1992**, *43*, 407–435.
- Pitera, J. W.; van Gunsteren, W. F. *Mol. Simulat.* **2002**, *28*, 45–65.
- Zacharias, M.; Straatsma, T. P.; McCammon, J. A. *J. Chem. Phys.* **1994**, *100*, 9025–9031.
- Pomès, R.; Eisenmesser, E.; Post, C. B.; Roux, B. *J. Chem. Phys.* **1999**, *111*, 3387–3395.
- Brooks, B. R.; Brucoleri, R. E.; Olafson, B. D.; States, D. J.; Swaminathan, S.; Karplus, M. *J. Comput. Chem.* **1983**, *4*, 187–217.
- Ferrenberg, A. M.; Swendsen, R. H. *Phys. Rev. Lett.* **1988**, *61*, 2635–2638.
- Ferrenberg, A. M.; Swendsen, R. H. *Phys. Rev. Lett.* **1989**, *63*, 1195–1198.
- Kumar, S.; Bouzida, D.; Swendsen, R. H.; Kollman, P. A.; Rosenberg, J. M. *J. Comput. Chem.* **1992**, *13*, 1011–1021.
- Jorgensen, W. L.; Severance, D. L. *J. Am. Chem. Soc.* **1990**, *112*, 4768–4774.
- Jorgensen, W. L.; Chandrasekhar, J.; Madura, J. D. *J. Chem. Phys.* **1983**, *79*, 926–935.
- Ryckaert, J.-P.; Ciccotti, G.; Berendsen, H. J. C. *J. Comput. Phys.* **1977**, *23*, 327–341.
- Landau, A. I. *J. Chem. Phys.* **2002**, *117*, 8607–8612.
- Feller, S. E.; Zhang, Y.; Paster, R. W.; Brooks, B. R. *J. Chem. Phys.* **1995**, *103*, 4613–4621.
- Hoover, W. G. *Phys. Rev. A* **1985**, *31*, 1695–1697.
- Lamoureux, G.; MacKerell, A.; Roux, B. *J. Chem. Phys.* **2003**, *119*, 5185–5197.
- Hummer, G.; Pratt, L.; Garcia, A. *J. Chem. Phys.* **1997**, *107*, 9275–9277.
- Villa, A.; Mark, A. E. *J. Comput. Chem.* **2002**, *23*, 548–553.
- Beutler, T. C.; Mark, A. E.; van Schaik, R. C.; Gerber, P. R.; van Gunsteren, W. F. *Chem. Phys. Lett.* **1994**, *222*, 529–539.
- Widom, B. *J. Chem. Phys.* **1963**, *39*, 2808–2812.
- Garde, S.; Hummer, G.; Paulaitis, M. E. *J. Chem. Phys.* **1998**, *108*, 1552–1561.
- Maccallum, J. L.; Tieleman, D. P. *J. Comput. Chem.* **2003**, *24*, 1930–1935.
- Gu, W.; Rahi, S. J.; Helms, V. *J. Phys. Chem. B* **2004**, *108*, 5806–5814.
- Chandler, D.; Weeks, J. D.; Anderson, H. C. *Science* **1983**, *220*, 787–794.
- Dixit, S. B.; Bhasin, R.; Rajasekaran, E.; Jayaram, B. *J. Chem. Soc., Faraday Trans.* **1997**, *93*, 1105–1113.
- CRC Handbook of Chemistry and Physics*, 83rd ed.; Lide, D. R., Ed.; CRC Press: New York, 2003.
- Chambers, C. C.; Hawkins, G. D.; Cramer, C. J.; Truhlar, D. G. *J. Phys. Chem.* **1996**, *100*, 16385–16398.